A reconnaissance teleseismic study of the upper mantle and transition zone beneath the Archean Slave craton in NW Canada

C.-G. Bank [a,*], M.G. Bostock [a], R.M. Ellis [a], J.F. Cassidy [b]

[a] *Department of Earth and Ocean Sciences, University of British Columbia, 2219 Main Mall, Vancouver B.C., Canada V6T 1Z4*
[b] *Pacific Geoscience Centre, Geological Survey of Canada, 4749–9860 West Saanich Road, Sidney, B.C., Canada V8L 4B2*

Abstract

The objective of this study is to investigate upper mantle structure below the Archean Slave craton, site of the oldest known rocks on Earth and numerous diamondiferous kimberlites, and thence to gain an understanding of early craton formation and kimberlite genesis. To this aim, a temporary array, consisting of 13 sites equipped with broadband seismometers, recorded teleseisms between November 1996 and May 1998. This data set has been augmented with recordings from the Yellowknife seismic array. Our three most robust observations and their interpretation are: (1) *P*-wave travel-time tomography reveals the oldest part of the craton, the Central Slave Basement Complex, to be underlain by the fastest seismic velocities, indicating that this block remains distinct well into mantle depths; (2) receiver function analysis requires only the Moho as major *S*-wave velocity discontinuity and points to a fairly constant crustal thickness throughout the Slave province; and (3) *SKS* splitting analysis shows little variation in delay times and fast polarization directions across the array, leading us to conclude that the present-day plate motion of North America is the primary cause for mantle fabric beneath the entire array. Furthermore, the data let us rule out the possibility that the Mackenzie plume had any seismologically detectable effect on the Slave lithosphere. More speculative results of our investigation, namely a possible genetic link between a low seismic velocity anomaly at depth with the overlying Lac de Gras kimberlite field, and a possible Archean origin of two shallow low-velocity anomalies, will require further investigation. © 2000 Elsevier Science B.V. All rights reserved.

Keywords: kimberlite; lithosphere; North American Craton; seismology; Slave Province; upper mantle

1. Introduction

Archean cratons form the nuclei of today's continents (Davis and Hegner, 1992, and references therein) and host economically important minerals and base metals. They are known to be underlain for the most part by 'cratonic keels' of relatively high seismic velocities and low densities (Jordan, 1978, 1988; Grand, 1994; Simons et al., 1999). The formation of these keels has been most successfully explained by the imbrication of subducted oceanic crust (Helmstaedt and Schulze, 1989; Abbott, 1991; de Wit et al., 1992; Hart et al., 1997; Bostock, 1998). However, several questions regarding Archean cratons and their mantle roots remain to be answered. These involve: (1) their

* Corresponding author. Tel: +1-604-822-2267;
fax: +1-604-822-6047.
E-mail address: bank@eos.ubc.ca (C.-G. Bank)

internal fabric and structure; (2) their stability with respect to plume interaction; and (3) the origin of diamondiferous kimberlites. An improved knowledge of the regional geophysical structure of the upper mantle beneath Archean cratons is desired as a contribution to this discussion.

The Slave province in northwest Canada is a craton of particular interest as it hosts the oldest known rocks on Earth and because of the occurrence of diamondiferous kimberlites. The latter implies the existence of a long-lived cratonic keel (e.g. Kirkley et al., 1991) which, at least in the western part of the Slave craton, is thought to have stabilized through underplating of subducted lithosphere (Bostock, 1998). The location of the study area is favourable with respect to the distribution of global seismicity, and the Yellowknife seismic array in the southwest corner of the province has provided detailed local information on mantle structure. For these reasons the Slave province is an ideal candidate for the seismological characterization of upper mantle below an Archean craton.

Using earthquake seismograms recorded on a portable broadband seismic array deployed across the Slave province, we have performed travel-time tomography, receiver function analysis, and *SKS* splitting analysis to provide a broad seismological view of the present-day upper mantle and transition zone below the Slave craton. Our results, in conjunction with supplementary xenolith, tectonic and other geophysical data from the interdisciplinary LITHOPROBE project (Clowes, 1997), provide important new information on present-day structure and long-term evolution of the upper mantle beneath this Archean province.

1.1. Tectonic overview

The Slave province is a well-preserved Archean block that lies within the northwestern part of the North American craton. The Archean rock record ranges from the oldest known intact rocks on Earth, the Acasta gneisses aged ca. 4.03 Ma (Bowring et al., 1990; Stern and Bleeker, 1998), to granitoids younger than 2.6 Ga. The province can be divided into a western and an eastern part (Fig. 1) on the basis of geochronology (Isachsen and Bowring, 1994), lead isotopes (Padgham and Fyson, 1992, and references therein), and ϵ_{Nd} values (Davis and Hegner, 1992), which leads to the following simplified model of its tectonic evolution (Kusky, 1989). The Hackett River (volcanic) Arc in the east (Fig. 1), aged 2.67 Ga, formed as an island arc by east-dipping subduction. The Contwoyto terrane developed as an accretionary complex in front of that arc, and together the pair collided with a microcontinent in the west, known as the Central Slave Basement Complex before 2.6 Ga. The Central Slave Basement Complex combines the Anton and Sleepy Dragon terranes of Kusky (1989) and was introduced by Bleeker et al. (1999) to account for the structural consistency observed throughout the south-central Slave province. We will hereafter refer to it as the CSBC.

The Slave province is bordered by two Proterozoic orogens, the Thelon orogen to the east and the Wopmay orogen to the west (Fig. 1). The Thelon orogen is a collisional type orogen that resulted from the convergence of the Slave province with the Rae province. This collision at ca. 1.9 Ga resulted from oblique east-dipping subduction and occurred along the Great Slave Lake shear zone (Hoffman, 1989). Postcollisional indentation at a later time interval (ca. 1.8 Ga) was accommodated by the conjugate Macdonald and Bathurst fault systems (Hoffman, 1989; Ritts and Grotzinger, 1994). (The Macdonald fault lies spatially close to the northeastern portion of the Great Slave Lake shear zone and is therefore not shown separately on Fig. 1.) The Wopmay orogen is an accretionary type orogenic belt thought to have developed in two stages. Westward-dipping subduction at 1.97 to 1.88 Ga lead to the accretion of the oceanic Hottah Arc and folding of the Coronation Supergroup which had been deposited along the passive margin. A reversal of subduction polarity formed the Great Bear Magmatic Zone (a continental magmatic arc) at 1.87 to 1.84 Ga. The Fort Simpson terrane docked post 1.84 Ga (Bowring and Grotzinger, 1992). Seismic reflection lines (Cook et al., 1999) show evidence that the oceanic lithospheres involved in these subduction events are still preserved beneath the southwestern Slave province.
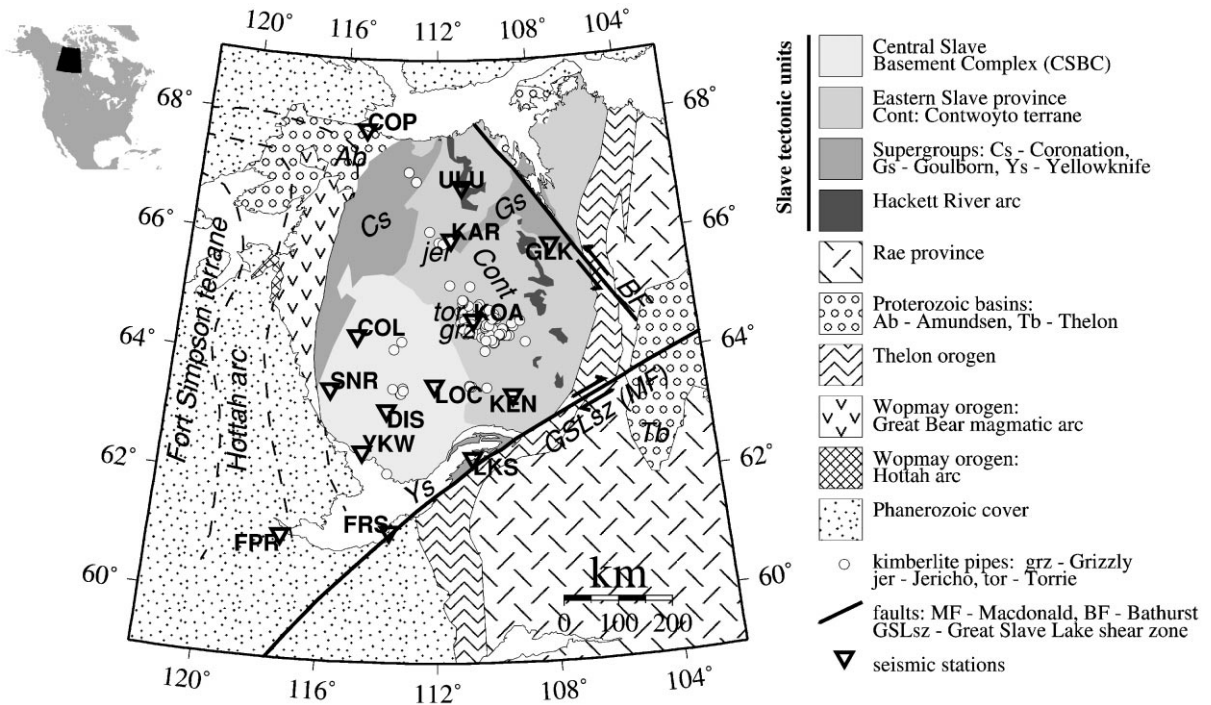
Fig. 1. Simplified tectonic map of the Slave craton and surrounding orogens. Geophysically inferred boundaries beneath the Proterozoic and Phanerozoic sediments in the west are shown as dashed lines.

The Mackenzie dykes are among the largest dyke swarms on Earth (Ernst et al., 1995), cutting the Slave craton at the surface as vertical sheets with a northwest-southeast trend. They were emplaced at 1.26 Ga during the same short time interval as the extrusion of Coppermine lavas in the northwest of the province. Both are thought to have originated through the impingement of a mantle plume below present-day Victoria Island [the focal point of the dykes lies at ca. 117°W, 71°N, see LeCheminant and Heaman (1989)].

Of economic importance, and of value to upper mantle studies, are the more than 150 kimberlite pipes that can be found scattered over the Slave province. None of these outcrops at the surface, but were detected either from aeromagnetic signatures or indicator minerals (Pell, 1997). Most kimberlites are non-micaceous (Group I) and are thought to have been derived from asthenospheric mantle, thereby sampling the whole lithospheric column shortly prior to the time of emplacement (Pell, 1997). Geochronological analyses show that

the kimberlites erupted at different times (Heaman et al., 1997); at Lac de Gras they were emplaced in the Late Cretaceous and the Early Tertiary, elsewhere in the eastern Slave they have been dated to mid-Jurassic and Cambrian times, and in the southwestern corner ages are Ordovician and Permian. Some of these kimberlites show high diamond potential, and Canada's first diamond mine (Ekati, location of seismic station KOA on Fig. 1) went into production in October 1998.

1.2. Data

From October 1996 to May 1998, a temporary seismic array consisting of 10 three-component broad-band instruments (NARS CSD20 data loggers and Güralp CMG-3/3T seismometers) and supplemented by five short-period instruments (Scintrex PRS-4 recorders and Mark L4-C seismometers) was deployed at mines and settlements on and around the Slave craton to record teleseisms. Deployment periods at individual sites varied

greatly in response to logistical support afforded by various mining camps. Additional data were retrieved from the Yellowknife seismic array operated by the Geological Survey of Canada. Broadband three-component recordings were acquired at the 14 locations indicated in Fig. 1.

Fig. 2 shows the distribution of events used in this study plotted on an equidistant projection centred on the Slave craton. Many events are suitable for travel-time tomography since only *P*-wave arrival times (both broad-band and short-period) are required. Analysis of converted phases in the coda of *P* requires a high signal-to-noise ratio on vertical and horizontal components, which generally is only afforded by larger events. The *SKS* phase, which provides a measure of vertically integrated lithospheric anisotropy, is best recorded at epicentral distances between 85° and 145° from large and deep events; the map indicates that most of these events over the period of the experiment originated in the southwest Pacific. Overall, event coverage is good except for azimuths between 185° and 235°.
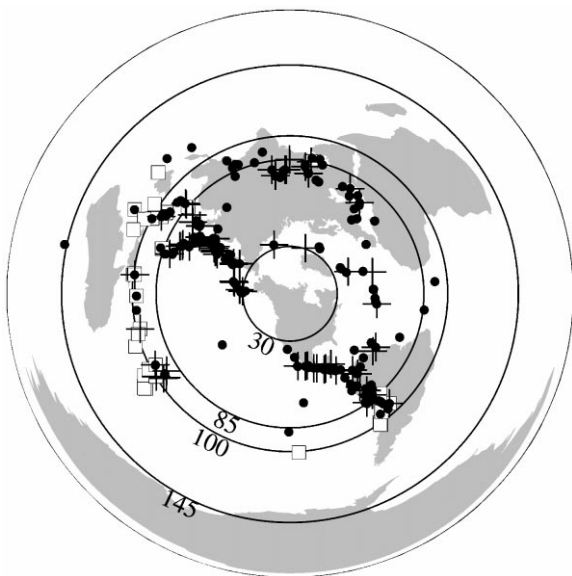

Fig. 2. Equidistant map of the world (epicentral distances to YKW in degrees) showing distribution of events used in this study. The three different symbols mark events used in the three different analyses: ●, 226 events used for travel-time tomography; +, 74 events used for receiver function analysis; and □, 34 events used for *SKS*-splitting analysis.

2. P-wave travel-time tomography

The method used to invert teleseismic travel-time residuals for variations in upper-mantle velocity is based on an algorithm developed by VanDecar (VanDecar 1991; VanDecar et al., 1995) for an elastically isotropic earth. Preprocessing involves the improvement of manually picked *P*-arrival times by multi-channel cross-correlation of vertical seismograms for a single event recorded at multiple stations (VanDecar and Crosson, 1990). These times are compared to predictions from the iasp91 reference Earth model (Kennett and Engdahl, 1991) to derive the travel-time residuals. Travel-time residuals from many events are then inverted for upper mantle slowness perturbations below the array. Contributions to the residuals from near source (e.g. earthquake mislocation and mistiming) and near-station structure (e.g. static corrections, lateral variations in velocity and thickness of crust) are accounted for separately from the slowness perturbations. The slowness perturbation field in the upper mantle beneath the array is parameterized by splines under tension fixed on a regular grid (VanDecar, 1991); in this study we used 37 000 knots spaced 35 km apart. Mapping of mantle structure from outside the region of interest into the bottom and sides of the model is a valid concern in inverting teleseismic delay times (see, e.g. Evans and Achauer, 1993). To mitigate this problem, we extended the grid well beyond the region of interest (>200 km or at least five layers of gridpoints).

The 226 events in Fig. 2 resulted in 1575 rays with a reasonable subsurface distribution. However, for any irregular event-station configuration we cannot expect to have uniform resolution throughout the entire model region. The size of the linear system discourages a formal construction of the resolution matrix, and a more qualitative approach has been taken here. We perform resolution tests by creating synthetic models, calculating the synthetic travel-time residuals along the ray paths for our experiment, and inverting those residuals for structure. For the 'checker-board' test shown in Fig. 3, the synthetic model consists of spikes of positive and negative anomalies spaced equidistantly at every sixth knot throughout the
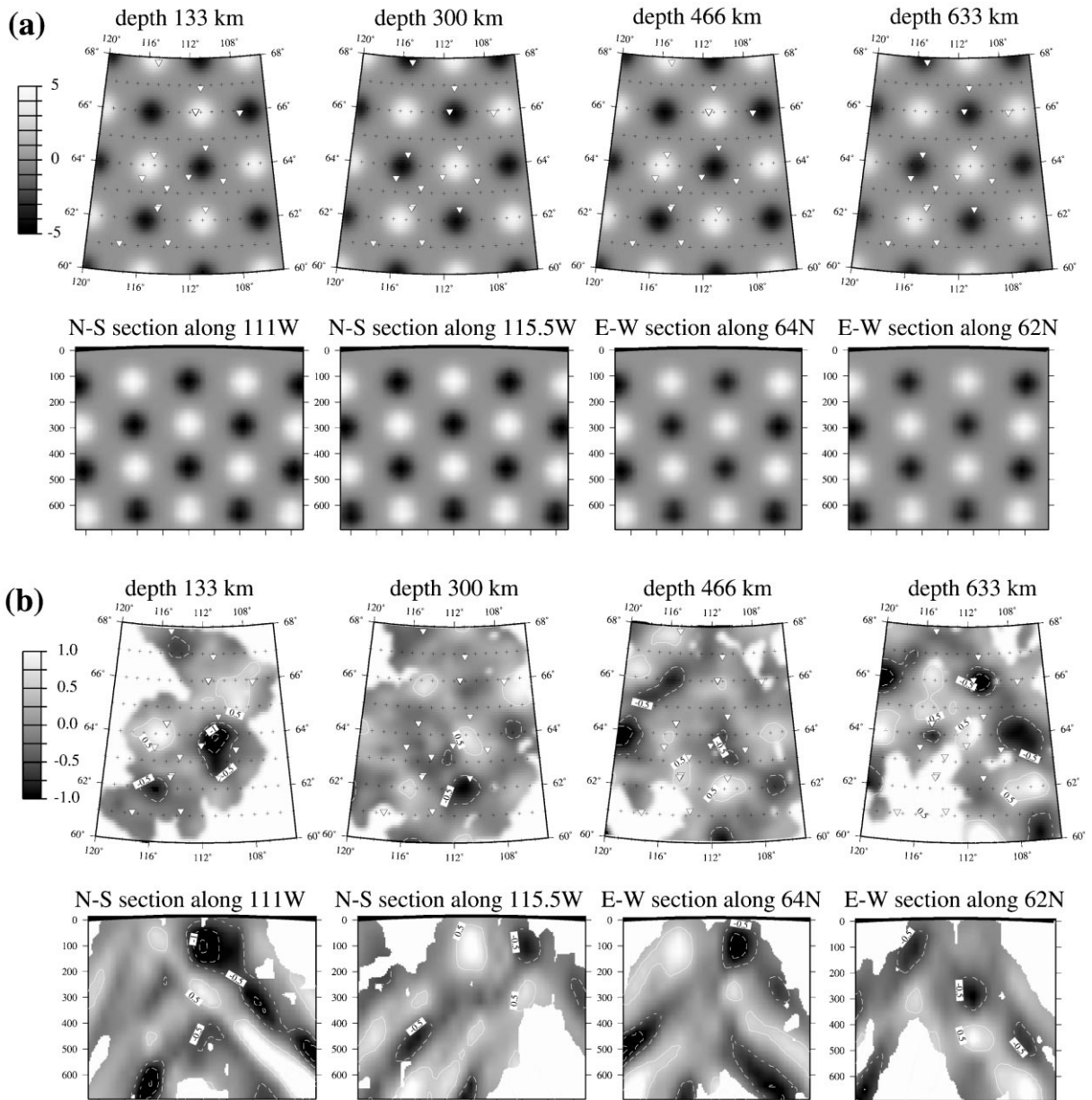
Fig. 3. 'Checkerboard' resolution test for travel-time tomography. Shown are the synthetic model (a) and the retrieved model (b). Note the different scales, they indicate slowness perturbation in percent. (Contours in the retrieved model are at 0.5% intervals, no 0% contour line.)

region of interest. A comparison of input and recovered models shows that we can expect a fairly good resolution beneath most of the array to depths as shallow as 90 km. Albeit some smearing is evident, particularly in the vertical slices, the locations of spikes are recovered throughout the upper mantle and transition zone (to 700 km depth), whereas their magnitudes are underesti-
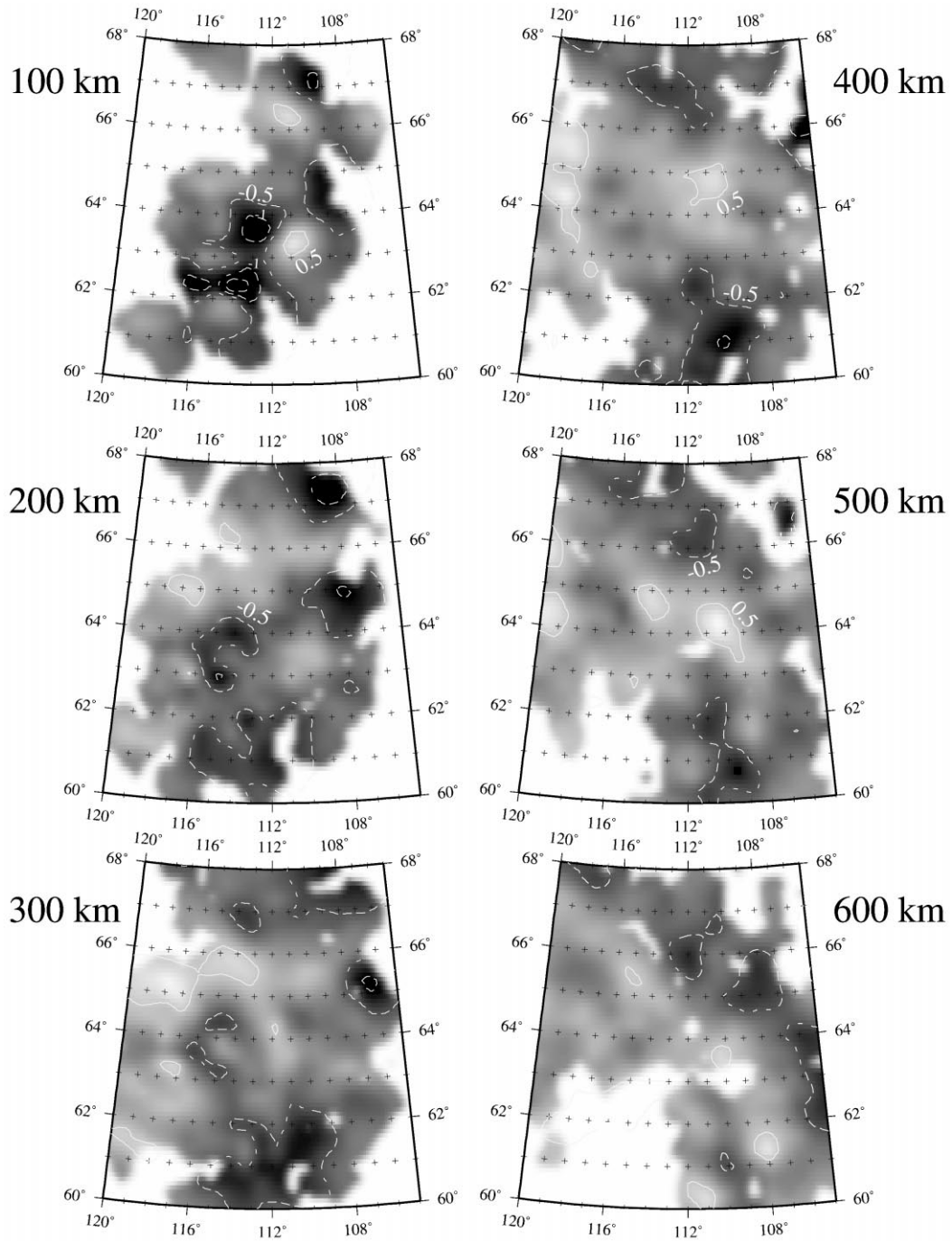
Fig. 4. Result of tomographic travel-time inversion. (a) Plan views. (b) Vertical cross-sections. Black areas (saturating at 1%) are fast and light coloured areas are slow with respect to iasp91; cells with low ray coverage are shaded to white; contours as in Fig. 3(b). The locations of seismic stations (▼) and the Slave craton (shaded area) are shown on the surface map together with the surface traces of the vertical cross-sections.
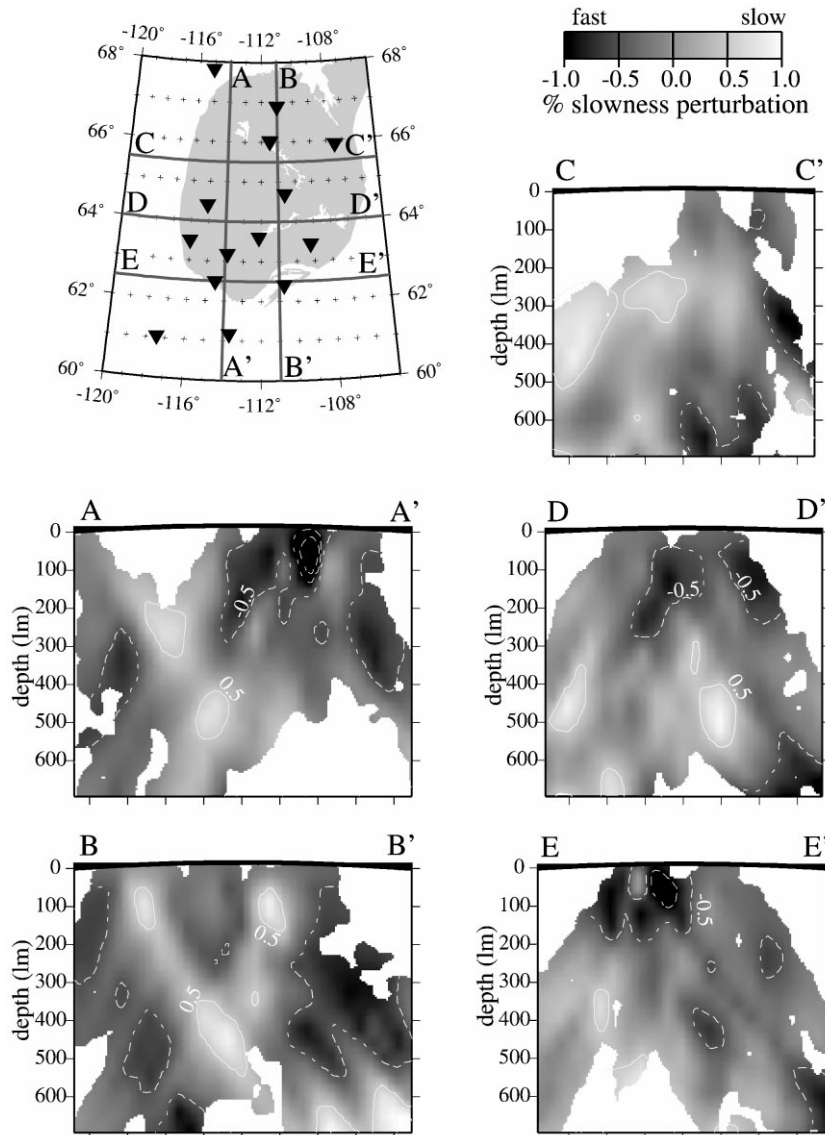
Fig. 4. (*continued*).

mated as a consequence, in part, of regularization imposed in the inversion. The vertical slices show anomalies at the sides of the model to be smeared along the ray paths while synthetic anomaly recovery at the centre of the volume is good. We may thus place confidence in the locations of anomalous structure seen in the central portion of the final model.

The preferred model, a compromise between the regularization level and the data misfit as determined from the construction of a tradeoff curve, is presented in Fig. 4. It, in conjunction with the station and event corrections, explains 94% of the travel-time perturbations, and varies in magnitude from -1.6% slowness perturbation at (62.3°N, 113.25°W, 100 km depth) to $+1.0\%$ slowness perturbation at (64.3°N, 110.25°W, 500 km depth). These extremes are centred on two

prominent features in the recovered model. First, we note higher than average seismic velocities in the southwest portion of the Slave province which extend to depths of 300 km (here we take the −0.5% slowness contour as diagnostic), and second, a low velocity anomaly (positive slowness variation above +0.5% slowness variation) ca. 100 km in diameter is confined between 350 and 600 km depth beneath the central Slave province. In addition to these two features, several other anomalies are also robust at various levels of regularization. These are high velocities in the shallow mantle also below the eastern part of the area, and two low velocity anomalies in the shallow mantle, centred at (66.3°N, 111°W, 133 km depth) and (63.3°N, 111°W, 133 km depth), respectively.

3. Simultaneous deconvolution for receiver functions

Velocity discontinuities in the crust and upper mantle may be discerned through analysis of *P*-to-*S* conversions recorded in the *P*-coda. We follow the approach of Bostock (1998) and transform the three-component displacement recordings into *P* and *S* wavefield components, and use *P* as the source estimate to be deconvolved from *S*. Simultaneous deconvolution improves the resolution as compared to a stacking of individual receiver functions because generally less damping is necessary to stabilize the deconvolution in the presence of noise (Gurrola et al., 1995). In addition, and to focus subtle arrivals originating at greater depths, the deconvolved seismograms are moveout-corrected for conversions at a range of trial depths (Vinnik et al., 1996).

We are unable to confidently constrain mantle lithospheric stratigraphy throughout the Slave craton as done by Bostock (1998) for the mantle beneath YKW because crustal multiples mask direct arrivals arising in the depth range between 120 and 250 km, and because the backazimuthal event distribution at individual stations is limited. Rather, we shall focus on the Mohorovičić discontinuity (Moho) and the global discontinuities at 410 and 660 km depth. The corresponding source normalized traces are shown in Fig. 5 The P_{M}s (*P*-

to-*S* conversion from the Moho) phase is identified beneath all stations on the Slave craton (ULU, KAR, GLK, KOA, COL, LOC, KEN and YKW) between 4.3 and 5.0 s after the direct *P* arrival; however if we consider the times at KAR and KEN as outliers due to few recorded events the time span for this arrival shrinks to 4.5 to 4.7 s, which corresponds to a variation in Moho depth between 37.2 and 39.8 km (see Table 1), assuming a crust with velocities given by iasp91. For stations on the margins of, or outside, the Slave province (COP, LKS, FRS and FPR) receiver functions show two symmetric peaks, the later arrival would define the Moho at 39–45.6 km. We note that the interpretation by Cook et al. (1999) of reflection data places the Moho at 40 km depth in the vicinity of Fort Providence (station FPR), close to our estimate using the later arrival. Generally, the P_{M}s arrival time appears later for stations outside the craton than for stations within, which may indicate a greater depth to the Moho. Cassidy and Bostock (1998) obtain similar results, in particular a well defined Moho peak and simple receiver functions on the Slave and more complicated receiver functions for the surrounding stations.

A majority of stations also show evidence of conversions from the 410 and 660 km discontinuities in the low-pass filtered (0.25–0.04 Hz) moveout corrected radial receiver functions (see Fig. 5). The arrival times for both phases are generally fast (by ca. 1 s) with respect to the expected iasp91 conversion times.

4. *SKS* splitting

Since the pioneering works by Vinnik and his co-workers (see, e.g. Kind et al., 1985, and references therein) *SKS* has been the preferred seismic phase to investigate anisotropy in the upper mantle, for a variety of reasons (see, e.g. Silver and Chan, 1991). The method used here was suggested by Silver and Chan (1988, 1991) and determines the two parameters (azimuth and delay) that best compensate for shear-wave splitting by minimizing: (1) the second eigenvalue of the covariance matrix formed from the reconstructed *SKS* wave; or (2) the energy on the transverse compo-
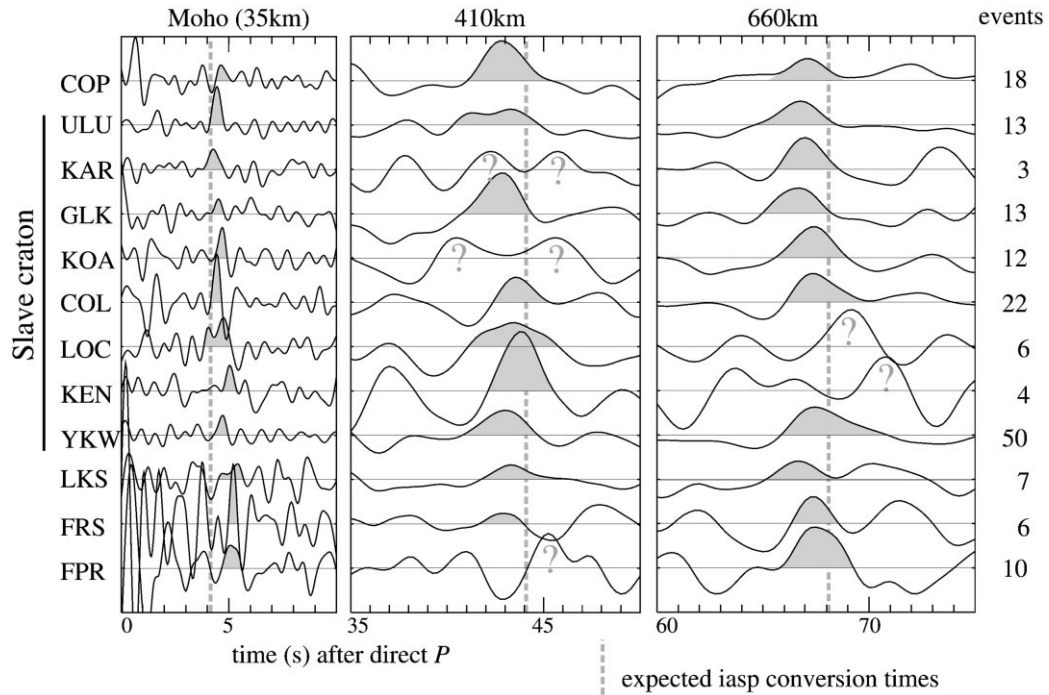
Fig. 5. Results of simultaneous deconvolution for receiver functions. The three panels show results for different depths after applying moveout corrections. Vertical dashed lines indicate expected arrival times of $P_M s$, $P_{410} s$ and $P_{660} s$ phases, respectively. Stations are sorted by latitude; number of events used for each station are given on the very right. Bandpass filters applied are 0.04–1.8 Hz for Moho traces and 0.04–0.25 Hz for others.

Table 1
Station locations and results of *SKS* splitting and simultaneous deconvolution

Station location			SKS splitting			Receiver function[a,b]				
Site	Lat. (°N)	Long. (°N)	Data	φ (°)	δt (s)	Data	Moho (s)	Moho (km)	410 (s)	660 (s)
COP	67.827	115.09	10	70 ± 7	0.4 ± 0.2	18	4.65	39.0	42.8	67.1
ULU	66.895	111.00	4	80 ± 10	0.8 ± 0.1	13	4.45	37.2	43.3	66.8
KAR	66.029	111.47	3	66 ± 9	0.7 ± 0.4	3	4.25	35.4	42.3?	66.9
GLK	65.920	107.46	3	71 ± 9	0.8 ± 0.5	13	4.50	37.6	42.8	66.6
KOA	64.692	110.63	8	43 ± 9	1.0 ± 0.2	12	4.70	39.4	40.5?	67.4
COL	64.411	115.10	9	50 ± 9	1.1 ± 0.3	22	4.45	37.2	43.5	67.3
LOC	63.611	112.12	–			6	4.75	39.8	43.4	69.1?
SNR	63.508	116.01	3	40 ± 2	1.5 ± 0.6	–				
KEN	63.436	109.21	3	65 ± 10	0.8 ± 0.5	4	5.04	42.4	43.8	70.8?
DIS	63.188	113.89	3	41 ± 11	0.8 ± 1.3	–				
YKW	62.493	114.51	24	56 ± 10	0.8 ± 0.3	50	4.70	39.4	43.0	67.4
LKS	62.406	110.74	4	65 ± 9	1.2 ± 0.4	7	5.40	45.6	43.3	66.6
FRS	61.175	113.68	5	59 ± 12	1.2 ± 0.3	6	5.20	43.8	42.8	67.3
FPR	61.050	117.44	5	64 ± 7	1.1 ± 0.2	10	5.05	42.5	45.2?	67.4

[a] iasp91 places Moho at 35 km depth, corresponding to a 4.2 s delay between direct P and P-to-S conversion; phase $P_{410} s$ has a 44.1 s delay and $P_{660} s$ has 68.1 s delay.
[b] Statistical error in time determination for Moho is ±0.05 s (or ±0.4 km); for 410 and 660 it is ±0.5 s.
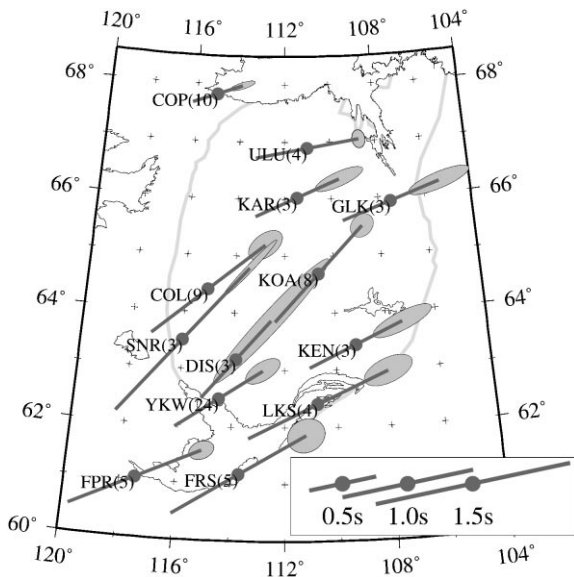
Fig. 6. Results of multi-event *SKS* splitting analysis. Bars point in the direction of the fast split wave; the length of the bars denote the delay time between split waves. The surface outline of the Slave craton is shown by the grey line. For each station the numbers of events used as well as the error ellipses are shown.

nent. Though the horizontal extent of anisotropy can be well constrained using this method, its vertical localization is more difficult to deduce. We kept only those data for which both methods produced consistent results and computed the averaged results for each station (see Fig. 6 and Table 1) using the stacking method of Wolfe and Silver (1998). Average splitting parameters show surprisingly little variation from station to station. The direction of the fast wave generally strikes southwest–northeast, averaging 60° (measured clockwise from north), and the delay times are of order ∼1 s for all stations. We note that our result for YKW is in general agreement with Silver and Chan (1991) and Bostock and Cassidy (1995) for that same location.

Most stations exhibit some scatter in individual splitting directions of ±15° for events from varying backazimuths. This observation is not unusual; a 90° periodicity in splitting parameters with backazimuth has been interpreted as evidence for multiple layering (e.g. Silver and Savage, 1994; Vinnik et al., 1994). A complex anisotropic stratification in the

mantle has been documented beneath Yellowknife (Bostock, 1998) and therefore we may expect some backazimuthal variation. Our event distribution lies within an 80° backazimuthal corridor extending from Tonga/Fiji to the Philippines (see Fig. 2), and so a possible 90° periodicity in splitting parameters cannot be detected. Clearly a longer observation interval would be necessary to obtain sufficient data to investigate this dependence in any detail. Nevertheless, the fact that all stations recorded the events used for SKS analysis from similar backazimuths affords the opportunity of assessing variations in mantle fabric across the array as we discuss in the following section.

5. Discussion

5.1. Crustal structure

Receiver functions show a clear Moho peak without large time variations for stations on the Slave craton (see Fig. 5, left panel). A mapping of these times to depth, assuming crustal velocities as defined in iasp91, indicates variations in Moho depth between 37 and 40 km within the craton (see Table 1), the average is 38 km. In contrast, Moho depths derived for stations off or on the edge of the craton are larger, 39–45, or 43 km on average. This is in accord with a global compilation by Durrheim and Mooney (1994), which found Archean crust to be generally < 40 km thick, and thinner than Proterozoic crust which usually is > 40 km. We acknowledge that our analysis is simplistic and does not consider lateral velocity variations, or changes in Moho transition width. Also, neither a refraction study across the southern Slave province and the Wopmay orogen (Fernandez Viejo et al., 1999) nor a reflection study in the same area (Cook et al., 1999) support any significant variation in Moho depth. Receiver functions for stations on the craton are generally simple. Our analysis does not capture the discontinuities imaged as prominent seismic reflections (Cook et al., 1999), as receiver functions sample *S*-velocity discontinuities and have a much lower frequency content (0.1–1.5 Hz) than seismic reflection studies that sample impedance contrasts

using *P*-waves at frequencies of 10–20 Hz. The only major *S*-wave velocity discontinuity required to explain the receiver functions is the continental Moho. More complex signatures observed at stations outside and at the edges of the craton may reflect the effects of Proterozoic orogeny such as a tectonic overprint of the Moho during collisional events, as has been suggested for Proterozoic [e.g. the Trans-Hudson Orogen, Hajnal et al. (1997)] as well as Phanerozoic orogens [e.g. the Alps, Pfiffner et al. (1990)]. The apparent lack of such structure within the Slave craton, albeit its assemblage through similar plate-tectonic processes, may support the notion of a ductile lower crust in the Archean (Bailey, 1999); however, a more targeted geophysical survey is necessary to justify this speculation.

Our results on crustal structure are only qualitative, insofar as no attempt to obtain detailed shear-wave velocity profiles at individual stations was made. The data set has been subjected to a more thorough analysis to obtain such velocity profiles and corresponding Moho depths (Cassidy and Bostock, 1998) the results of which will be presented elsewhere.

5.2. Lithospheric thickness and structure

Preliminary magnetotelluric results (Jones and Ferguson, 1997; Clowes, 1997) reveal an electrically isotropic lithosphere beneath the CSBC and adjacent Great Bear magmatic arc that sits between lithosphere exhibiting large anisotropy to both the east and west. The base of the electrical lithosphere, as evidenced by an increase in conductivity, is found at 250–300 km beneath the CSBC and thins across the Great Bear magmatic arc to ~150 km. Petrological studies of xenoliths from the Jericho pipe (close to our station KAR, see Fig. 1) have made use of geothermobarometry and determined a petrological boundary at 190 km depth (Kopylova et al., 1998), which separates porphyroclastic peridotites and magmatic rocks below from coarse garnet peridotite and eclogite above, and is further characterized by an inflection in the calculated paleogeotherm. They interpret this boundary to be the base of the lithosphere at the time of kimberlite emplacement at ca. 172 Ma.

Another study, by MacKenzie and Canil (1998), on xenoliths from the Torrie kimberlite pipe (in the vicinity of station KOA, see Fig. 1, ca. 65 Ma emplacement, Dante Canil, personal communication) estimated a similar lithospheric thickness. Boyd and Canil (1997) determined a lithospheric thickness of at least 200 km for the Grizzly pipe (also close to KOA). Assuming that no mantle-root destructive event has taken place since emplacement of the kimberlites these thickness estimates should be valid at present.

Our tomographic results can be brought into general agreement with these lithospheric thickness estimates if we adopt the ~0.5% slowness contour as significant, because it lies above any slowness variation that could arise from noise in the data. In the central, better resolved regions of the model this boundary generally occurs near ~250±50 km although some lateral variations do occur. In particular the highest velocities are found beneath the CSBC, that is, the oldest portion of the Slave craton [see comparison of tomographic results with surface tectonics in Fig. 7(a)] which suggests that this lithospheric block may be distinct from adjacent terranes to a depth of ~150 km, that is, well into the mantle.

Two shallow low velocity anomalies have been identified as robust features in the tomographic inversion. Both lie within the Slave lithosphere and are located between the Hackett river arc and the CSBC (Fig. 7a). Kusky (1993) proposes that the Slave lithosphere is built up by imbricated slabs of Archean oceanic crust and lithosphere together with trapped wedges of fertile (undepleted) mantle. His hypothesis explains the formation of late- to postkinematic granitoid suites by decompression melting of these mantle wedges [see Kusky and Polat (1999), for a detailed discussion of this process]. In an extension of this proposal we speculate that the low velocity anomalies visible in the tomographic image may be trapped regions of fertile mantle, mantle material which retained a lherzolitic composition with associated lower seismic velocity than the surrounding (harzburgitic) lithosphere. We note that the velocity variation recovered in our travel-time inversion is of the order as that measured on xenoliths of fertile versus depleted mantle affinity (e.g. Jordan, 1979;
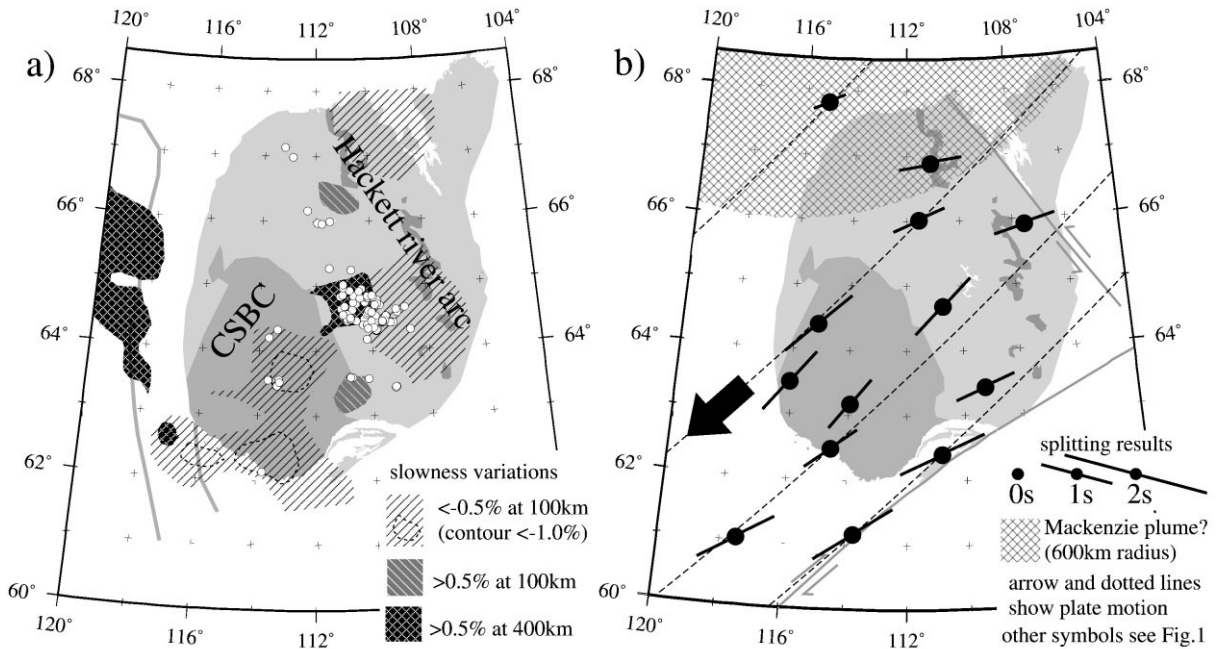
Fig. 7. Comparison of our results to surface tectonic features. The area of the Slave craton is shaded to light grey. (a) Results from travel-time tomography overlie tectonics. Kimberlite locations (○) and aeromagnetic boundaries (western boundary of Slave and western boundary of Great Bear magmatic arc as grey lines) have been added for clarity. (b) Results from SKS splitting analysis related to tectonics. The figure also shows the Great Slave Lake shear zone (with the spatially close Macdonald fault), the Bathurst fault, traces of the North American plate motion (black dashed lines, Minster and Jordan, 1978) and the estimated region of vertical magma flow in the Mackenzie dykes (cross-hatched area).

Kern, 1993; Kern et al., 1996). Griffin et al. (1999) note that garnet concentrates recovered from a kimberlite 100 km south of Lac de Gras, situated at the northern rim of one of the shallow seismic anomalies, indicate relatively fertile lherzolite at a shallow depth (above 150 km). Clearly, more xenolith studies that confirm the existence of fertile mantle material within the Slave lithosphere are required to validate this speculation.

Analysis of receiver functions has shown the peaks defining the discontinuities at 410 and 660 km to be shifted to earlier times (∼1 s) at all stations relative to iasp91 and we therefore infer that the upper mantle underlying the Slave craton is faster than the global average, consistent with the high absolute velocities generally accorded to cratonic lithosphere. Because the shifts for the $P_{410}s$ and $P_{660}s$ phases are for the most part similar, the thickness of the transition zone does not appear to differ from the global average, a

conclusion in agreement with previous studies carried out using the Yellowknife seismic array (Bostock and Cassidy, 1997).

5.3. Origin of anisotropy

Shear-wave splitting measured from teleseismic shear-waves has been ascribed to preferential alignment of anisotropic mantle minerals, mainly olivine. As the cause of this alignment, some favour preserved lithospheric fabric [see, e.g. review article by Silver (1996)] and others prefer current plate motion (e.g. Vinnik et al., 1992). In the first case it is assumed that deformation is vertically coherent and that the polarization direction mimics the direction of tectonic deformation. In the second case the polarization direction aligns generally with the direction of plate motion in the hot-spots reference frame. However, Bormann et al. (1996) and Fouch et al. (2000) show that topography at

the base of the lithosphere may locally deflect the asthenospheric flow caused by the movement of the plate.

Our results indicate similar splitting parameters at all stations, and may be compared to the direction of present-day plate motion and main tectonic features in Fig. 7(b). For the southern stations (e.g. FRS and LKS) an ambiguity exists regarding the possible origin of splitting as the observed fast polarization direction coincides well with both the plate motion direction and the prominent Great Slave Lake shear zone located a few tens of km to the southeast. However, the splitting directions at more northerly stations, in particular GLK, are highly oblique to the conjugate Bathurst fault system, also responsible for accommodating indentation of the Slave craton into the Rae craton near 1.86 Ga. It is unlikely that anisotropic fabric developed prior to the Bathurst fault system would not have been disrupted by the indentation since continent–continent collision is the most catastrophic process represented by plate tectonics. We therefore suggest that the rather uniform pattern of fast polarization directions is more strongly influenced by present-day absolute plate motion than past lithospheric deformation history. A slight variation in fast directions between neighbouring stations (e.g. KOA and KEN) may be caused by variations in internal lithospheric fabric (Bostock, 1998) or topography on the base of the lithosphere. Note however that the difference ($\sim 20°$) is comparable to the estimated error at individual stations.

5.4. Influence of the Mackenzie plume

An investigation of magnetic fabric in the Mackenzie dykes (Ernst and Baragar, 1992) demonstrated a pronounced change in pattern ~ 600 km away from the focal point of the dykes. This was interpreted as a change from dominantly vertical to horizontal dyke emplacement, and postulated to represent the outer limit of lithospheric erosion by the Mackenzie plume. Helmstaedt and Gurney (1995) accepted this interpretation and suggested that the Mackenzie plume was a mantle-root destructive event which essentially destroyed the cratonic keel of the northern Slave province.

Our results do not support such a large-scale destruction of the Slave lithosphere by the Mackenzie plume. We performed a synthetic experiment to test the potential resolution of an extensive low velocity anomaly in the uppermost mantle to the north of the Slave craton, as might be expected had the high-velocity cratonic keel been removed by plume interaction. The synthetic anomaly had a radius of 600 km around the focal point of the Mackenzie dykes [as proposed by Ernst and Baragar (1992)], a slowness perturbation of +1.5%, and extended from 50 to 200 km depth. Synthetic travel times were computed and noise added (using a level slightly higher than shown by the data). The result showed that the southern limit was recovered as were low velocities in the shallow mantle within the defined radius. The observed model, in contrast, indicates velocities slightly higher than the background model in the north. Furthermore, *SKS* splitting delay times and fast polarization directions for the northern stations COP and ULU do not deviate from values at the other stations, thus suggesting that a rapid change in upper mantle fabric does not occur. Furthermore, receiver functions at the northern stations COP and ULU show no evidence for upper mantle of lower velocity to the north of the Slave craton, since *Ps* conversions from the 410 and 660 km discontinuities arrive at times comparable to those of most other stations of the array. Other evidence against such large-scale erosion of thick lithosphere by mantle plumes is supplied from geodynamic arguments. Davies (1994) provided quantitative estimates of plume erosion in lithosphere of varying thickness. His calculations show that only above the plume conduit is the temperature gradient sufficiently strong to cause significant erosion; thermal inertia over the plume head in general is insufficient to cause substantial lithospheric thinning.

5.5. Speculations on an origin for the Lac de Gras kimberlite cluster

The cluster of kimberlites near the Lac de Gras area at the centre of the Slave craton is underlain by a well-resolved low-velocity anomaly at 350–600 km depth (see comparison in Fig. 7a).

Moreover, analysis of *Ps* conversions from the 410 km discontinuity at station KOA, which overlies this anomaly, fails to reveal a clear pulse which would suggest structural heterogeneity at transition zone depths (see Fig. 5). Note that the receiver function at station KAR situated just to the north of the anomaly also shows a more complex waveform at 40–45 s after direct *P* but this is based on fewer (3 versus 12) waveforms and may not be reliable. The geographic correspondence of seismological observations with the kimberlite field prompts speculation into a genetic association. A link between mantle plumes/diapirs and kimberlites has been suggested by various authors (e.g. Green and Gueguen, 1974; Crough et al., 1980; Haggerty, 1994). If such a direct causative relation is invoked here, we must take into consideration the ages of kimberlites from the Lac de Gras area [late Cretaceous to early Tertiary, see Pell (1997)], and necessitate a coherent motion of this anomaly and underlying transition zone for at least 50 Ma. Some precedent for this is provided through a tomographic study by VanDecar et al. (1995), who interpreted a low-velocity anomaly beneath the Paraná basin in Brazil as a remnant of the Tristan da Cunha plume head which had translated coherently with the overlying plate since Cretaceous time. To summon the same interpretation here clearly requires that the relative uniformity of *SKS*-splitting parameters shown in Fig. 6 be ascribed to a mechanism other than absolute plate motion.

6. Concluding remarks

Analysis of the data set acquired in this study has led to three important conclusions. The location of the high velocity region in the shallow mantle beneath the CSBC suggests that this tectonic block remains distinct into mantle depths. Simple receiver functions found for most stations situated within the internal portions of the Slave province point to a relatively constant crustal thickness near 36–39 km. The coherency in splitting directions across the array favours an origin in absolute plate motion over fossilized lithospheric anisotropy. Other interesting observations present themselves, notably a possible complexity in deep upper mantle and transition zone structure below the Lac de Gras kimberlite field suggests a possible genetic association; however a comprehensive evaluation of this interpretation will await a more detailed survey.

References

Abbott, D., 1991. The case for accretion of the tectosphere by buoyant subduction. Geophys. Res. Lett. 18 (4), 585–588.

Bailey, R.C., 1999. Gravity-driven continental overflow and Archaean tectonics. Nature 398, 413–415.

Bleeker, W., Ketchum, J.W.F., Jackson, V.A., Villeneuve, M., 1999. The Central Slave Basement Complex, part I: its structural topology and autochthonous cover. Can. J. Earth Sci. 36, 1083–1109.

Bormann, P., Grünthal, G., Kind, R., Montag, H., 1996. Upper mantle anisotropy beneath central Europe from *SKS* wave

splitting: effects of absolute plate motion and lithosphere–asthenosphere boundary topography? J. Geodyn. 22, 11–32.

Bostock, M.G., 1998. Mantle stratigraphy and evolution of the Slave province. J. Geophys. Res. 103 B9, 21183–21200.

Bostock, M.G., Cassidy, J.F., 1995. Variations in *SKS* splitting across western Canada. Geophys. Res. Lett. 22 (1), 5–8.

Bostock, M.G., Cassidy, J.F., 1997. Upper mantle stratigraphy beneath the southern Slave craton. Can. J. Earth Sci. 34, 577–587.

Bowring, S.A., Grotzinger, J.P., 1992. Implications of new chronostratigraphy for tectonic evolution of Wopmay orogen, Northwest Canadian Shield. Am. J. Sci. 292, 1–20.

Bowring, S.A., Housh, T.B., Isachsen, C.E., 1990. The Acasta Gneisses: remnant of Earth's early crust. In: Newsom, H.E., Jones, J.H. (Eds.), Origin of the Earth. Oxford University Press, New York, pp. 319–343.

Boyd, F.R., Canil, D., 1997. Peridotite xenoliths from the Slave craton, Northwest Territories. Paper presented at Seventh Annual V.M. Goldschmidt Conference, Tucson, AZ, USA, 2–6 June.

Cassidy, J.F., Bostock, M.G., 1998. Crustal structure of the Archean Slave craton from receiver function studies. In: Abstracts for Annual Meeting, 18–20 May. Geological Association of Canada/Mineralogical Association of Canada, Québec City, Canada, p. A28.

Clowes, R.M. (Ed.), 1997. Lithoprobe Phase V Proposal — Evolution of a Continent Revealed. Lithoprobe Secretariat, University of British Columbia, Vancouver, Canada.

Cook, F.A., van der Velden, A.J., Hall, K.W., Roberts, B.J., 1999. Frozen subduction in Canada's Northwest Territories: Lithoprobe deep lithospheric reflection profiling of the western Canadian Shield. Tectonics 18 (1), 1–24.

Crough, S.T., Morgan, W.J., Hargraves, R.B., 1980. Kimberlites: their relation to mantle hotspots. Earth Planet. Sci. Lett. 50, 260–274.

Davies, G.F., 1994. Thermomechanical erosion of the lithosphere by mantle plumes. J. Geophys. Res. 99 B8, 15709–15722.

Davis, W.J., Hegner, E., 1992. Neodymium isotopic evidence for the tectonic assembly of Late Archean crust in the Slave province, northwest Canada. Contrib. Mineral. Petrol. 111, 493–504.

Durrheim, R.J., Mooney, W.D., 1994. Evolution of the Precambrian lithosphere: seismological and geochemical constraints. J. Geophys. Res. 99 B8, 15359–15374.

Ernst, R.E., Baragar, W.R.A., 1992. Evidence from magnetic fabric for the flow pattern of magma in the Mackenzie giant radiating dyke swarm. Nature 356, 511–513.

Ernst, R.E., Head, J.W., Parfitt, E., Grosfils, E., Wilson, L., 1995. Giant radiating dyke swarms on Earth and Venus. Earth-Sci. Rev. 39, 1–58.

Evans, J.R., Achauer, U., 1993. Teleseismic velocity tomography using the ACH method: theory and application to continental-scale studies. In: Iyer, H.M., Hirahara, K. (Eds.), Seismic Tomography: Theory and Practice. Chapman and Hall, London, UK, pp. 319–360.

Fernandez Viejo, G., Clowes, R.M., Amor, J.R., 1999. Imaging the lithospheric mantle in northwestern Canada with seismic wide-angle reflections. Geophys. Res. Lett. 26 (18), 2809–2812.

Fouch, M.J., Fischer, K.M., Parmentier, E.M., Wysession, M.E., Clarke, T.J., 2000. Shear wave splitting, continental keels, and patterns of mantle flow. J. Geophys. Res. 105 B3, 6255–6276.

Grand, S.P., 1994. Mantle shear structure beneath the Americas and surrounding oceans. J. Geophys. Res. 99 B6, 11591–11621.

Green, H.W., Gueguen, Y., 1974. Origin of kimberlite pipes by diapiric upwelling in the upper mantle. Nature 249, 617–620.

Griffin, W.L., Doyle, B.J., Ryan, C.G., Pearson, N.J., O'Reilly, S.Y., Natapov, L., Kivi, K., Kretschmar, U., Ward, J., 1999. Lithosphere structure and mantle terranes: Slave Craton, Canada. Proc. 7th Int. Kimb. Conf., Red Roof Design, Cape Town. pp. 299–306

Gurrola, H., Baker, G.E., Minster, J.B., 1995. Simultaneous time-domain deconvolution with application to the computation of receiver functions. Geophys. J. Int. 120, 537–543.

Haggerty, S.E., 1994. Superkimberlites: a geodynamic diamond window to the Earth's core. Earth Planet. Sci. Lett. 122, 57–69.

Hajnal, Z., Nemeth, B., Clowes, R.M., Ellis, R.M., Spence, G.D., Burianyk, M.J.A., Asudeh, I., White, D.J., Forsyth, D.A., 1997. Mantle involvement in lithospheric collision: seismic evidence from the Trans-Hudson Orogen, western Canada. Geophys. Res. Lett. 24 (16), 2079–2082.

Hart, R.J., Tredoux, M., de Wit, M.J., 1997. Refractory trace elements in diamond inclusions: further clues to the origins of the ancient cratons. Geology 25 (12), 1143–1146.

Heaman, L.M., Kjarsgaard, B., Creaser, R.A., Cookenboo, H.O., Kretschmar, U., 1997. Multiple episodes of kimberlite magmatism in the Slave province North America. In: Lithoprobe Report vol. 56. Lithoprobe Secretariat,, University of British Columbia, Vancouver, Canada, pp. 14–17.

Helmstaedt, H.H., Gurney, J.J., 1995. Geotectonic controls of primary diamond deposits: implications for area selection. J. Geochem. Explor. 53, 125–144.

Helmstaedt, H., Schulze, D.J., 1989. Southern African kimberlites and their mantle sample: implications for Archaean tectonics and lithosphere evolution. In: Ross, J. (Ed.), Kimberlites and Related Rocks. Blackwell, Cambridge, MA, pp. 358–368.

Hoffman, P.F., 1989. Precambrian geology and tectonic history of North America. In: Bally, A.W., Palmer, A.R. (Eds.), The Geology of North America — An overview. Geol. Soc. Am, Boulder, CO, pp. 447–512.

Isachsen, C.E., Bowring, S.A., 1994. Evolution of the Slave craton. Geology 22, 917–920.

Jones, A.G., Ferguson, I.J., 1997. Results from 1996 MT studies along Snorcle profiles 1 and 1a. In: Lithoprobe Report vol. 56. Lithoprobe Secretariat, University of British Columbia, Vancouver, Canada, pp. 42–47.

Jordan, T.H., 1978. Composition and development of the continental tectosphere. Nature 274, 544–548.

Jordan, T.H., 1979. Mineralogies, densities and seismic veloci-

ties of garnet lherzolites and their geophysical implications. In: Boyd, F.R., Meyer, H.O.A. (Eds.), The Mantle Sample: Inclusions in Kimberlites and Other Volcanics. AGU, Washington, DC, pp. 1–14.

Jordan, T.H., 1988. Structure and formation of the continental tectosphere. J. Petrol. Special Lithosphere Issue, 11–37.

Kennett, B.L.N., Engdahl, E.R., 1991. Traveltimes for global earthquake location and phase identification. Geophys. J. Int. 105, 429–465.

Kern, H., 1993. P- and S-wave anisotropy and shear-wave splitting at pressure and temperature in possible mantle rocks and their relation to the rock fabric. Phys. Earth Planet. Inter. 78, 245–256.

Kern, H., Burlini, L., Ashchepcov, I.V., 1996. Fabric-related seismic anisotropy in upper-mantle xenoliths: evidence from measurements and calculations. Phys. Earth Planet. Inter. 95, 195–209.

Kind, R., Kosarev, G.L., Makeyeva, L.I., Vinnik, L.P., 1985. Observations of laterally inhomogenous anisotropy in the continental lithosphere. Nature 318, 358–361.

Kirkley, M.B., Gurney, J.J., Levinson, A.A., 1991. Age, origin and emplacement of diamonds: scientific advances in the last decade. Gems Gemol. 27 (1), 2–25.

Kopylova, M.G., Russell, J.K., Cookenboo, H., 1998. Upper-mantle stratigraphy of the Slave craton, Canada: insights into a new kimberlite province. Geology 26 (4), 315–318.

Kusky, T.M., 1989. Accretion of the Archean Slave province. Geology 17 (1), 63–67.

Kusky, T.M., 1993. Collapse of Archean orogens and the generation of late- to postkinematic granitoids. Geology 21 (10), 925–928.

Kusky, T.M., Polat, A., 1999. Growth of granite–greenstone terranes at convergent margins, and stabilization of Archean cratons. Tectonophysics 305, 43–73.

LeCheminant, A.N., Heaman, L.M., 1989. Mackenzie igneous events, Canada: middle Proterozoic hotspot magmatism associated with ocean opening. Earth Planet. Sci. Lett. 96, 38–48.

MacKenzie, J.M., Canil, D., 1998. Composition and thermal evolution of cratonic mantle beneath the central Archean Slave Province, NWT, Canada. Contrib. Mineral. Petrol. 134, 313–324.

Minster, J.B., Jordan, T.H., 1978. Present-day plate motions.. J. Geophys. Res. 83, 5331–5354.

Padgham, W.A., Fyson, W.K., 1992. The Slave Province: a distinct Archean craton. Can. J. Earth Sci. 29, 2072–2086.

Pell, J.A., 1997. Kimberlites in the Slave craton, Northwest Territories, Canada. Geosci. Canada 24 (2), 77–90.

Pfiffner, O.A., Frei, W., Valasek, P., Stäuble, M., Levato, L., DuBois, L., Schmidt, S.M., Smithson, S.B., 1990. Crustal shortening in the Alpine orogen: results from deep seismic reflection profiling in the eastern Swiss Alps, line NFP 20-East. Tectonics 9 (6), 1327–1355.

Ritts, B.D., Grotzinger, J.P., 1994. Depositional facies and detrital composition of the Paleoproterozoic Et-Then Group, N.W.T., Canada: sedimentary response to intracratonic indentation. Can. J. Earth Sci. 31, 1763–1778.

Silver, P.G., 1996. Seismic anisotropy beneath the continents: probing the depths of Geology. Annu. Rev. Earth Planet. Sci. 24, 385–432.

Silver, P.G., Chan, W.W., 1988. Implications for continental structure and evolution from seismic anisotropy. Nature 335, 34–39.

Silver, P.G., Chan, W.W., 1991. Shear wave splitting and subcontinental mantle deformation. J. Geophys. Res. 96 B10, 16429–16454.

Silver, P.G., Savage, M.K., 1994. The interpretation of shear-wave splitting parameters in the presence of two anisotropic layers. Geophys. J. Int. 119, 949–963.

Simons, F.J., Zielhuis, A., van der Hilst, R.D., 1999. The deep structure of the Australian continent from surface wave tomography. Lithos 48, 17–43.

Stern, R.A., Bleeker, W., 1998. Age of the world's oldest rocks refined using Canada's SHRIMP: The Acasta gneiss complex, Northwest Territories, Canada. Geosci. Canada 25 (1), 27–31.

VanDecar, J.C., 1991. Upper-mantle structure of the Cascadia subduction zone from non-linear teleseismic travel-time inversion. PhD Thesis, University of Washington, Seattle, USA.

VanDecar, J.C., Crosson, R.S., 1990. Determination of teleseismic relative phase arrival times using multi-channel cross-correlation and least squares. Bull. Seismol. Soc. Am. 80 (1), 150–169.

VanDecar, J.C., James, D.E., Assumpçãao, M., 1995. Seismic evidence for coherent flow of the crust and upper mantle below South America since the breakup of Gondwana. Nature 378, 25–31.

Vinnik, L.P., Makeyeva, L.I., Milev, A., Usenko, A.Yu., 1992. Global patterns of azimuthal anisotropy and deformations in the continental mantle. Geophys. J. Int. 111, 433–447.

Vinnik, L., Krishna, V.G., Kind, R., Bormann, P., Stammler, K., 1994. Shear wave splitting in the records of the German Regional Seismic Network. Geophys. Res. Lett. 21 (6), 457–460.

Vinnik, L.P., Green, R.E.W., Nicolaysen, L.O., Kosarev, G.L., Petersen, N.V., 1996. Deep seismic structure of the Kaapvaal craton. Tectonophysics 262, 67–75.

Wessel, P., Smith, W.H.F., 1991. Free software helps map and display data. Eos. Trans. AGU 72, 441–446.

de Wit, M., Roehring, C., Hart, R.J., Armstrong, R.A., de Ronde, C.E.J., Green, R.W.E., Tredoux, M., Peberdy, E., Hart, R.A., 1992. Formation of an Archaean continent. Nature 357, 553–562.

Wolfe, C.J., Silver, P.G., 1998. Seismic anisotropy of oceanic upper mantle: shear wave splitting methodologies and observations. J. Geophys. Res. 103 B1, 749–771.